Chiral orbital current and anomalous magnetic moment in gapped graphene

Mikito Koshino
Department of Physics, Tohoku University, Sendai, 980-8578, Japan
(Received 27 May 2011; revised manuscript received 24 July 2011; published 12 September 2011)

We present a low-energy effective-mass theory to describe a chiral orbital current and an anomalous magnetic moment in graphenes with a band gap and related materials. We explicitly derive a quantum-mechanical current distribution in general Bloch electron systems, which describes a chiral current circulation supporting the magnetic moment. We apply the formulation to gapped graphene monolayer, bilayer, and ABC-stacked multilayers to show that the chiral current is opposite between different valleys, and the corresponding magnetic moment accounts for valley splitting of Landau levels. In a gapped bilayer and ABC multilayer graphenes, in particular, the valley-dependent magnetic moment is responsible for huge paramagnetic susceptibility at low energy, which enables a full valley polarization up to relatively high electron densities. The formulation also applies to the gapped surface states of a three-dimensional topological insulator, where the anomalous current is related to the magnetoelectric response in a spatially modulated potential.

DOI: 10.1103/PhysRevB.84.125427 PACS number(s): 81.05.ue, 75.20.−g, 75.70.Ak

I. INTRODUCTION

The magnetic moment in an electronic system consists of two distinct factors due to the spin and orbital motion of electrons. In solids, the spin magnetic moment is enhanced by an anomalous factor caused by the orbital effect, resulting in an increase in the g factor.[1,2] Graphene[3–5] has an intriguing counterpart of spin, which is associated with valley pseudospins, i.e., the degree of freedom corresponding to different points in the Brillouin zone called K_+ and K_- valleys. Specifically, when the band gap is opened by an asymmetric potential breaking the sublattice symmetry, the graphene electrons have an anomalous magnetic moment, which is opposite in different valleys and is similar to a real spin.[6–8] Generally, the anomalous magnetic moment is closely related to the geometric nature of the Bloch band and has been argued about in relation to the Berry phase.[9–13] Previously, we calculated the orbital susceptibility in gapped monolayer and bilayer graphenes and showed that the susceptibility near the $K_\pm$ point, where the dispersion is quadratic, is contributed from the Pauli paramagnetism caused by the valley pseudospin.[8]

In this paper, to understand the physical origin of the pseudospin magnetic moment and to investigate the pseudospin magnetic moment in various electronic structures other than quadratic dispersion, we develop a general low-energy effective-mass theory to describe the anomalous current density supporting the magnetic moment. We explicitly derive a quantum-mechanical current distribution in general Bloch electron systems, which describes a chiral current circulation for each eigenstate. Using the formula, we actually calculate the valley-dependent chiral current in a gapped graphene monolayer, bilayer,[14–17] and ABC-stacked multilayers.[18–20] The valley-dependent magnetic moment exactly gives the valley splitting of Landau levels, generalizing our previous results limited to the quadratic dispersion.[8] In particular, in the gapped bilayer[8] and ABC multilayers, the valley splitting and diverging density of states at the band bottom result in a huge paramagnetic susceptibility, enabling a full valley polarization up to a relatively high electron density on the order of 10^{12} cm^{-2} at a magnetic field of ~ 1 T.

The formulation also allows inclusion of the external potential field within the low-energy approximation and, thus, is useful for investigating the chiral current in disordered systems and also finite systems bound by the potential barrier. It also applies to the gapped surface states of the three-dimensional topological insulator, where the anomalous current describes the magnetoelectric response in a spatially modulated potential.[21–24]

This paper is organized as follows. In Sec. II, we present the general effective-mass description of the anomalous current density for Bloch electrons. We apply this to asymmetric monolayer, bilayer, and ABC-multilayer graphenes in Secs. III–V, respectively, to describe the chiral current circulation, magnetic moment, and valley splitting of Landau levels. In Sec. VI, we calculate the magnetic susceptibility and argue about the role of the anomalous magnetic moment. In Sec. VII, we describe the current distribution in a spatially modulated external potential and formulate it in terms of a response function analogous to the Hall conductivity. The conclusion is given in Sec. VIII.

II. ANOMALOUS ORBITAL CURRENT

We consider a Bloch electron system described by an effective-mass Hamiltonian matrix $\mathcal{H}_{mm'}(\mathbf{p})$, where $\mathbf{p}$ is the crystal momentum and m and m' are band indices. We assume that the Hamiltonian is diagonalized at $\mathbf{p} = 0$ as

$$\mathcal{H}_{mm'}(0) = \varepsilon^0_m \delta_{mm'}, \tag{1}$$

and, for simplicity, that there is no degeneracy at $\mathbf{p} = 0$. In the presence of external potential $V(\mathbf{r})$, the effective-mass wave function $\mathbf{F}(\mathbf{r})$ obeys the Schrödinger equation,

$$\sum_{m'} \mathcal{H}_{mm'}(\mathbf{p}) F_{m'}(\mathbf{r}) = [\varepsilon - V(\mathbf{r})] F_m(\mathbf{r}), \tag{2}$$

where $\mathbf{p} = -i\hbar\nabla$ and ε is the eigenenergy. We assume $|V| \ll |\varepsilon^0_m - \varepsilon^0_{m'}|$ so that the states of different bands are not strongly mixed.

We focus on an eigenstate near $\varepsilon = \varepsilon^0_n$ of the particular band n. Then, the wave function has its amplitude mainly on

F_n. By the first-order perturbation, the amplitude at $F_{m\neq n}$ can be written in terms of F_n as

$$F_m(\mathbf{r}) \approx \frac{\mathcal{H}_{mn}(\mathbf{p})}{\varepsilon_n^0 - \varepsilon_m^0} F_n(\mathbf{r}). \tag{3}$$

The Schrödinger equation, Eq. (2), then becomes

$$\left[\mathcal{H}_n^{(\mathrm{eff})}(\mathbf{p}) + V(\mathbf{r})\right] F_n(\mathbf{r}) = \varepsilon F_n(\mathbf{r}), \tag{4}$$

with the effective Hamiltonian,

$$\mathcal{H}_n^{(\mathrm{eff})}(\mathbf{p}) = \mathcal{H}_{nn}(\mathbf{p}) + \sum_{m\neq n} \frac{\mathcal{H}_{nm}(\mathbf{p})\mathcal{H}_{mn}(\mathbf{p})}{\varepsilon_n^0 - \varepsilon_m^0}. \tag{5}$$

Correspondingly, we can define the effective velocity operator,

$$v_n^{\mu(\mathrm{eff})} = \frac{\partial \mathcal{H}_n^{(\mathrm{eff})}(\mathbf{p})}{\partial p_\mu}, \tag{6}$$

and the local current density operator,

$$\begin{aligned} j_n^{\mu(\mathrm{eff})}(\mathbf{R}) = -\frac{e}{2}\left\{v_n^{\mu(\mathrm{eff})}, \delta(\mathbf{r}-\mathbf{R})\right\} = -\frac{e}{2}\Bigg[\left\{v_{nn}^{\mu}, \delta(\mathbf{r}-\mathbf{R})\right\} \\ + \sum_{m\neq n} \frac{1}{\varepsilon_n^0 - \varepsilon_m^0}\Big\{\big(v_{nm}^{\mu}\mathcal{H}_{mn} \\ + \mathcal{H}_{nm} v_{mn}^{\mu}\big), \delta(\mathbf{r}-\mathbf{R})\Big\}\Bigg], \end{aligned} \tag{7}$$

where $\{a,b\} = ab + ba$ is the anticommutator and

$$v_{mm'}^{\mu} = \frac{\partial \mathcal{H}_{mm'}(\mathbf{p})}{\partial p_\mu}. \tag{8}$$

$j_n^{\mu(\mathrm{eff})}$ actually covers only part of the total current density even in the low-energy limit. The original current density operator is given by

$$j^{\mu}(\mathbf{R}) = -\frac{e}{2}\left\{v^{\mu}, \delta(\mathbf{r}-\mathbf{R})\right\}, \tag{9}$$

where v^μ is a matrix defined by Eq. (8). The expectation value of j^μ for a given state $\mathbf{F}$ near ε_n^0 is written as

$$\begin{aligned} \langle j^{\mu}(\mathbf{R})\rangle &= \sum_{mm'} \int d\mathbf{r}\, F_m^*(\mathbf{r})[j^{\mu}(\mathbf{R})]_{mm'} F_{m'}(\mathbf{r}) \\ &\approx \int d\mathbf{r}\, F_n^*(\mathbf{r}) j_n^{\mu}(\mathbf{R}) F_n(\mathbf{r}). \end{aligned} \tag{10}$$

In the second equation, we used Eq. (3) and defined

$$\begin{aligned} j_n^{\mu}(\mathbf{R}) = -\frac{e}{2}\Bigg[&\left\{v_{nn}^{\mu}, \delta(\mathbf{r}-\mathbf{R})\right\} \\ &+ \sum_{m\neq n} \frac{1}{\varepsilon_n^0 - \varepsilon_m^0}\Big(\left\{v_{nm}^{\mu}, \delta(\mathbf{r}-\mathbf{R})\right\}\mathcal{H}_{mn} \\ &+ \mathcal{H}_{nm}\left\{v_{mn}^{\mu}, \delta(\mathbf{r}-\mathbf{R})\right\}\Big)\Bigg] = j_n^{\mu(\mathrm{eff})}(\mathbf{R}) \\ &- \frac{e}{2}\sum_{m\neq n} \frac{1}{\varepsilon_n^0 - \varepsilon_m^0}\left\{v_{nm}^{\mu}[\delta(\mathbf{r}-\mathbf{R}), \mathcal{H}_{mn}] + \mathrm{H.c.}\right\}. \end{aligned} \tag{11}$$

j_n^μ is not equivalent to $j_n^{\mu(\mathrm{eff})}$ since $\mathcal{H}_{mn}$ and $\delta(\mathbf{r}-\mathbf{R})$ do not generally commute. As shown in the following, the second term, called the anomalous current in the following, is responsible for the chiral current circulation in gapped graphenes.

A similar argument is available for the orbital magnetic moment. The operator of the magnetic moment perpendicular to the layer is defined as

$$m = -\frac{e}{2c}(x v^y - y v^x). \tag{12}$$

Similar to Eq. (10), the expectation value of m for a state of band n can be written as

$$\langle m\rangle \approx \int d\mathbf{r}\, F_n^*(\mathbf{r}) m_n F_n(\mathbf{r}), \tag{13}$$

where m_n is the effective magnetic moment,

$$\begin{aligned} m_n = &-\frac{e}{2c}\left(x v_n^{y(\mathrm{eff})} - y v_n^{x(\mathrm{eff})}\right) \\ &-\frac{e\hbar}{2c}\sum_{m\neq n}\frac{1}{i}\frac{v_{nm}^x v_{mn}^y - v_{nm}^y v_{mn}^x}{\varepsilon_n^0 - \varepsilon_m^0}. \end{aligned} \tag{14}$$

The first term is the magnetic moment given by the orbital current $j_n^{\mu(\mathrm{eff})}$. The second term is the extra magnetic moment coming from the anomalous current and coincides with the expression of magnetic moment, which enhances the g factor in a conventional semiconductor physics.[1,2]

While we include a diagonal scalar potential $V(\mathbf{r})$ in the above argument, an off-diagonal potential generally is possible in systems, such as graphene with a random vector potential. As long as the potential term enters the Hamiltonian in the form of $\mathcal{H}_{mn} + V_{mn}(\mathbf{r})$, as in the random vector potential for graphene, the expression of the chiral current Eq. (11) is not influenced since V_{mn} commutes with $\delta(\mathbf{r}-\mathbf{R})$ and does not alter the velocity operator v_{mn}^μ.

III. MONOLAYER GRAPHENE

Graphene is composed of a honeycomb network of carbon atoms, where a unit cell contains a pair of sublattices, denoted by A and B. Low-energy electronic states are described by the effective Hamiltonian,[25–33]

$$\mathcal{H}(\mathbf{p}) = \begin{pmatrix} \Delta & v p_- \\ v p_+ & -\Delta \end{pmatrix}, \tag{15}$$

where $p_\pm = \xi p_x \pm i p_y$, $\xi = \pm$ is the valley index corresponding to the K_ξ point in the Brillouin zone, and $\mathbf{p}$ is the momentum measured from K_ξ. The matrix works on a two-component envelope wave function $[F_A(\mathbf{r}), F_B(\mathbf{r})]$ at the A and B sublattices, respectively. The diagonal terms $\pm\Delta$, opening the energy gap at the Dirac point, are given by the potential asymmetry between A and B sites, which, for instance, can arise in a certain substrate material.[34,35] The band velocity is $v \approx 1 \times 10^6$ m/s.

The surface states of the three-dimensional topological insulator of the Bi_2Se_3 family is also described by a similar Hamiltonian to Eq. (15), where (p_x, p_y) is rotated to $(p_y, -p_x)$.[23,24] The rotation of vector $\mathbf{p}$ is compensated by the spinor rotation and does not affect the following argument. There is only a single valley index, and the diagonal term Δ appears

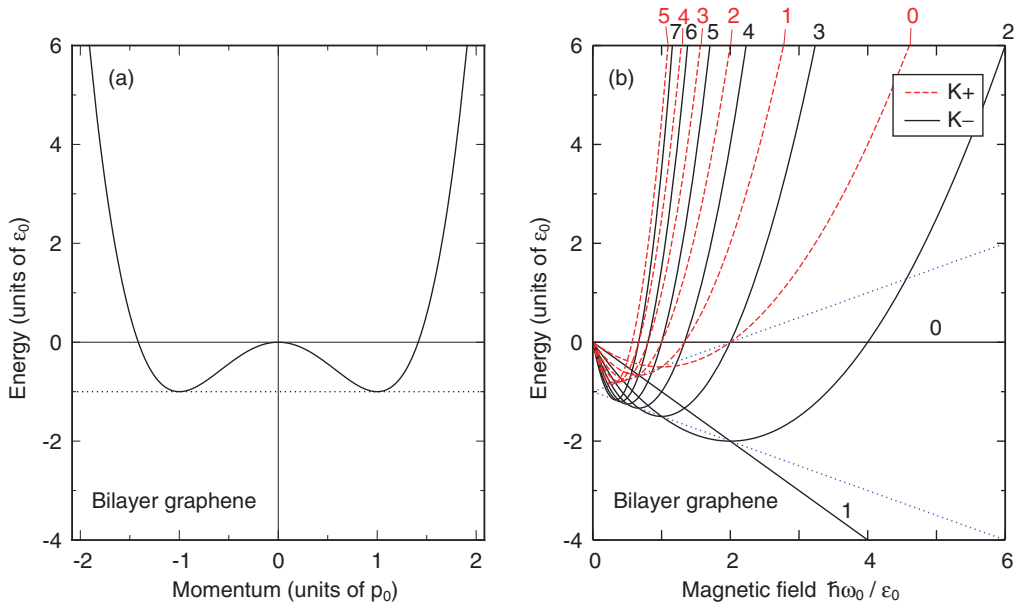

FIG. 1. (Color online) (a) Low-energy dispersion of gapped bilayer graphene given by Eq. (27). (b) Landau level spectrum of Eq. (39) with some small n's, plotted against the magnetic field. Dashed (red) and solid (black) lines represent the valleys $\xi = +$ and $-$, respectively. Numbers assigned to the curves indicate Landau level index n. A pair of dotted slopes represents the energy of the band bottom shifted by pseudospin Zeeman energy, i.e., $-\varepsilon_0 \pm \hbar\omega_0/2$. At $\Delta = 0.1$ eV, the characteristic energy scale is $\varepsilon_0 = 13$ meV, and the magnetic field for $\hbar\omega_0/\varepsilon_0 = 1$ is 7.6 T.

only when the time-reversal symmetry is broken, for instance, by attaching a ferromagnetic material.[21,22]

We assume $\Delta > 0$ and consider a state near the electron band bottom $\varepsilon = \Delta$. Then, the wave amplitude is concentrated mainly on the first component $F \equiv F_A$. The reduced Hamiltonian for F excluding the constant energy becomes,

$$\mathcal{H}^{(\mathrm{eff})}(\mathbf{p}) = \frac{p^2}{2m^*}, \tag{16}$$

with the effective mass,

$$m^* = \frac{\Delta}{v^2}. \tag{17}$$

Applying Eq. (11), the local current density is written as

$$\langle \mathbf{j}(\mathbf{r}) \rangle = -\frac{e\hbar}{m^*}\,\mathrm{Im}(F^*\boldsymbol{\nabla} F) - \xi\frac{e\hbar}{2m^*}(-\mathbf{e}_z \times \boldsymbol{\nabla})|F|^2, \tag{18}$$

where $\boldsymbol{\nabla} = (\partial/\partial x, \partial/\partial y, 0)$ and $\mathbf{e}_z = (0,0,1)$. The first term is the usual current density, corresponding to $j^{(\mathrm{eff})}$ of Eq. (11). The second term is the anomalous component and is denoted as $\mathbf{j}_c$ in the following. It flows perpendicularly to the gradient of density $|F|^2$, and thus, it circulates on a closed loop and does not contribute to the electron transport. The direction is opposite between $\xi = \pm$. It is written in terms of the equivalent local magnetic moment $\boldsymbol{\mu}$ as

$$\begin{aligned} \langle \mathbf{j}_c(\mathbf{r}) \rangle &= c\boldsymbol{\nabla} \times \boldsymbol{\mu}(\mathbf{r}), \\ \boldsymbol{\mu}(\mathbf{r}) &= -\xi\frac{e\hbar}{2m^*c}|F|^2\mathbf{e}_z. \end{aligned} \tag{19}$$

For the valence-band electron, a similar calculation shows that the first term of Eq. (18) flips the sign, while the second term remains unchanged.

The expression of the magnetic moment operator, Eq. (14), becomes

$$m = -\frac{e}{2m^*c}(xp_y - yp_x) - \xi\frac{e\hbar}{2m^*c}, \tag{20}$$

where the first and second terms correspond to those of Eq. (18), respectively. The second term, now denoted as m_c, is the magnetic moment induced by the anomalous current and coincides with the integral of $\boldsymbol{\mu}(\mathbf{r})$ in Eq. (19) over the space. It should be noted that m_c is constant regardless of the details of the wave function. This is analogous to the spin magnetic moment of the bare electron system with ξ being the spin index, while in graphene, this is mimicked by the valley-dependent chiral orbital current. The expression of m_c agrees with an intrinsic magnetic moment in the semiclassical picture, which is regarded as the self-rotation of the wave packet.[6]

The valley pseudospin magnetic moment m_c produces the pseudospin Zeeman energy in the presence of a magnetic field, and this accounts for the valley splitting of Landau levels in graphene.[8] This can be checked by considering the Hamiltonian in a uniform external field $\mathbf{B}$, or $\mathcal{H}(\boldsymbol{\pi})$ in Eq. (15), where $\boldsymbol{\pi} \equiv \mathbf{p} + e\mathbf{A}/c$ with the vector potential $\mathbf{A}$ giving $\mathbf{B} = \boldsymbol{\nabla} \times \mathbf{A}$. Noting the relation $[\pi_x, \pi_y] = -i\hbar eB/c$, the reduced Hamiltonian for the A site near $\varepsilon = \Delta$ is written as[8]

$$\mathcal{H}^{(\mathrm{eff})}(\boldsymbol{\pi}) \approx \frac{v^2}{2\Delta}\pi_-\pi_+ = \hbar\omega_c\left(\hat{n} + \frac{1}{2} + \frac{\xi}{2}\right), \tag{21}$$

where $\omega_c = eB/(m^*c)$, $\pi_\pm = \xi\pi_x \pm i\pi_y$, $\hat{n} = a^\dagger a$, and $a = (2\hbar eB/c)^{-1/2}(\pi_x - i\pi_y)$ is the annihilation operator of the Landau level and we used the relation $\pi^2 = (2\hbar eB/c)(\hat{n} + 1/2)$. The term depending on ξ is the pseudospin Zeeman energy, and it actually coincides with $-m_c \cdot B$. In graphene,

the pseudospin Zeeman splitting is equal to the Landau level spacing so that the nth Landau level at valley K_+ has the same energy $(n+1)$-th level at K_-.

The two terms in the current distribution of Eq. (18) can be distinguished by a change in the two-dimensional mirror reflection,

$$F(\mathbf{r}) \to F'(\mathbf{r}) \equiv F(\mathbf{r}'), \tag{22}$$

where $\mathbf{r} = (x,y)$ and $\mathbf{r}' = (-x,y)$. Let $\mathbf{j}(\mathbf{r})$ and $\mathbf{j}'(\mathbf{r})$ be the expectation values of the current density for wave functions F and F', respectively. Each current component changes with either $s = \pm$ in

$$\begin{pmatrix} j'_x(\mathbf{r}') \\ j'_y(\mathbf{r}') \end{pmatrix} = s \begin{pmatrix} -j_x(\mathbf{r}) \\ j_y(\mathbf{r}) \end{pmatrix}, \tag{23}$$

or equivalently,

$$\mathbf{r}' \times \mathbf{j}'(\mathbf{r}') = -s\mathbf{r} \times \mathbf{j}(\mathbf{r}). \tag{24}$$

In Eq. (18), the first term $\mathbf{j}^{(\mathrm{eff})}$ yields to $s = +$, i.e., the current map is just mirror reflected in the same way as $\mathbf{r}$. This is a natural consequence, since $\mathcal{H}^{(\mathrm{eff})}$ is invariant in the mirror reflection.

The second term $\mathbf{j}_c$ has the opposite sign $s = -$, or $\mathbf{j}'_c$ goes against the mirror reflection of $\mathbf{j}_c$ and can be called chiral in this sense. In gapped graphene, having this term may look counterintuitive since the system is originally mirror symmetric with respect to a line containing an AB bond. But this real reflection exchanges valleys $\xi = \pm$ at the same time in addition to Eq. (22) so that $\mathbf{j}_c$, then, simply is mirror reflected as it should be. Therefore, the chiral term is necessarily accompanied by factor ξ.

Two current components also behave differently in the effective time-reversal operation $F \to F^*$ within a single valley. The first term obviously reverses in this operation as a consequence of the effective time-reversal symmetry for $\mathcal{H}^{(\mathrm{eff})}$. The second term only depends on the absolute value of the wave amplitude and, thus, remains unchanged in the same operation. But it reverses in the real time-reversal operation, which switches $\xi = \pm$. We will see that the same argument will apply to bilayer graphene as well.

IV. BILAYER GRAPHENE

Bilayer graphene[14–17] is a pair of graphene layers arranged in AB (Bernal) stacking and includes A_1 and B_1 atoms on layer 1 and A_2 and B_2 on layer 2.[36–43] The states at B_1 and A_2 are coupled by $\gamma_1 \approx 0.39$ eV.[44] The low-energy states are described by the Hamiltonian matrix for the basis $(|A_1\rangle, |B_1\rangle, |A_2\rangle, |B_2\rangle)$,[36,37]

$$\mathcal{H}(\mathbf{p}) = \begin{pmatrix} \Delta & vp_- & 0 & 0 \\ vp_+ & \Delta & \gamma_1 & 0 \\ 0 & \gamma_1 & -\Delta & vp_- \\ 0 & 0 & vp_+ & -\Delta \end{pmatrix}, \tag{25}$$

where Δ describes potential asymmetry between layers 1 and 2 (not A and B sites), which gives rise to an energy gap.[36–40,42,45,46] Experimentally, the potential asymmetry can be induced by applying an electric field perpendicular to the layer,[15–17,47,48] and the asymmetry as large as $\Delta \sim 0.1$ eV was actually observed in spectroscopic measurements.[15,47,48] For simplicity, we neglected the trigonal warping effect due to the extra band parameter.[36,41]

Let us assume $\Delta > 0$ in the following. At $\mathbf{p} = 0$, the Hamiltonian gives four eigenenergies,

$$\begin{aligned} \varepsilon_1^0 &= -\sqrt{\gamma_1^2 + \Delta^2}, \qquad \varepsilon_2^0 = -\Delta, \\ \varepsilon_3^0 &= \Delta, \qquad \varepsilon_4^0 = \sqrt{\gamma_1^2 + \Delta^2}. \end{aligned} \tag{26}$$

We consider a state near the conduction-band bottom $\varepsilon = \varepsilon_3^0$, of which wave amplitude is mostly concentrated on the first component $F_{A1} \equiv F$. The effective Hamiltonian for F is[37]

$$\begin{aligned} \mathcal{H}^{(\mathrm{eff})}(\mathbf{p}) &\approx \frac{1}{2\Delta}\frac{v^4p^4}{\gamma_1^2} - 2\Delta\frac{v^2p^2}{\gamma_1^2} \\ &\equiv \frac{p^4}{4m_0p_0^2} - \frac{p^2}{2m_0}, \end{aligned} \tag{27}$$

where the energy is measured from $\varepsilon = \Delta$ and

$$m_0 = \frac{\gamma_1^2}{4v^2\Delta}, \qquad p_0 = \hbar k_0 = \frac{\sqrt{2}\Delta}{v}. \tag{28}$$

The term with p^2 comes from the off-diagonal elements $\mathcal{H}_{34}$ and $\mathcal{H}_{31}$ in the Hamiltonian matrix diagonalized for $p = 0$. To have the p^4 term, in Eq. (5), we need the higher-order term for the off-diagonal matrix element between $j = 2$ and 3; i.e., use instead of $\mathcal{H}_{32}$,

$$\tilde{\mathcal{H}}_{32} = \mathcal{H}_{32} + \sum_{m=1,4} \mathcal{H}_{3n}\frac{1}{\varepsilon_3^0 - \varepsilon_n^0}\mathcal{H}_{n2}. \tag{29}$$

The dispersion is plotted in Fig. 1(a). It is a nonmonotonic function of p, and the band minimum appears at off-center momentum $p = p_0$ and energy $\varepsilon = -\varepsilon_0$, where

$$\varepsilon_0 = \frac{2\Delta^3}{\gamma_1^2}. \tag{30}$$

For instance, the asymmetric energy of $\Delta = 0.1$ eV gives $\varepsilon_0 = 13$ meV. The density of states is given by

$$D(\varepsilon) = g_s g_v \frac{m_0}{2\pi\hbar^2}\frac{1}{\sqrt{1+\varepsilon/\varepsilon_0}} \times \begin{cases} 0 & (\varepsilon < -\varepsilon_0), \\ 2 & (-\varepsilon_0 < \varepsilon < 0), \\ 1 & (\varepsilon > 0), \end{cases} \tag{31}$$

where $g_s = g_v = 2$ is the spin and valley degeneracies.

The local current density of Eq. (11) is written in the same level of approximation as

$$\langle \mathbf{j}(\mathbf{r}) \rangle = \mathrm{Im}\,\mathbf{u} + \xi(-\mathbf{e}_z \times \mathrm{Re}\,\mathbf{u}), \tag{32}$$

where the vector $\mathbf{u}$ is defined by

$$\begin{aligned} u_\mu = &-\frac{e\hbar}{2m_0}\frac{1}{k_0^2}\sum_{v=x,y}\left[2(\partial_v F^*)\partial_\mu(\partial_v F) - \partial_\mu\left(F^*\partial_v^2 F\right)\right] \\ &+\frac{e\hbar}{m_0}F^*\partial_\mu F. \end{aligned} \tag{33}$$

The second component of $\langle \mathbf{j}(\mathbf{r}) \rangle$ is the chiral current and is expressed as

$$\langle \mathbf{j}_c(\mathbf{r}) \rangle = c\nabla \times \boldsymbol{\mu}(\mathbf{r}),$$
$$\boldsymbol{\mu}(\mathbf{r}) = \xi \mathbf{e}_z \frac{e\hbar}{2m_0 c} \left\{ -\frac{1}{k_0^2} \left[|\nabla F|^2 - \mathrm{Re}(F^* \nabla^2 F) \right] + |F|^2 \right\}. \tag{34}$$

The equivalent magnetic moment $\boldsymbol{\mu}(\mathbf{r})$ now depends on F and its derivative. The magnetization of Eq. (14) becomes

$$m = -\frac{e}{2c}(x v^{y(\mathrm{eff})} - y v^{x(\mathrm{eff})}) - \xi \frac{e\hbar}{m_0 c} \left(\frac{p^2}{p_0^2} - \frac{1}{2} \right). \tag{35}$$

The second term m_c is the valley magnetic moment induced by the chiral current. The valley-splitting energy at the band bottom can be estimated by inserting $p = p_0$,

$$2|m_c(p_0)|\, B = \frac{\hbar e B}{m_0 c} \equiv \hbar\omega_0. \tag{36}$$

The effective g factor for this pseudospin splitting is given by $g^* = 2m/m_0$ where m is the bare electron mass. g^* is proportional to Δ, and it approximates 30 at $\Delta = 0.1$ eV.

When the valley splitting exceeds ε_F, the system is fully valley polarized with a single kind of chiral particle. Using the density of states of Eq. (31), the condition for full valley polarization is estimated in the low B-field limit,

$$n < n_{\mathrm{crit}} = g_s \frac{1}{\pi} \frac{\Delta}{\hbar v} \sqrt{\frac{2eB}{c\hbar}}, \tag{37}$$

where n is the electron density. We have $n_{\mathrm{crit}} \approx 5 \times 10^{11}$ cm^{-2} at $\Delta = 0.1$ eV and $B = 1$ T. For the gapped monolayer graphene, the condition is

$$n < n_{\mathrm{crit}} = g_s \frac{eB}{h}, \tag{38}$$

which is approximately 5×10^{10} cm^{-2} at $B = 1$ T. In the bilayer, the critical density is proportional to $\sqrt{B}$ rather than B, and thus, the valley polarization is achieved in much lower magnetic fields than in the monolayer in a small electron density. This property is caused by the divergence of the density of states at the band bottom.

Similar to the monolayer, the valley splitting of Landau levels in asymmetric bilayer graphene[16,36,49] is correctly given by the pseudospin Zeeman energy due to the magnetic moment m_c. The original Hamiltonian in a magnetic field is given by Eq. (25) with $\mathbf{p}$ replaced by $\boldsymbol{\pi}$. Near $\varepsilon = \Delta$, it is reduced to

$$\begin{aligned} \mathcal{H}^{(\mathrm{eff})}(\boldsymbol{\pi}) &\approx \frac{1}{2\Delta} \frac{(v\pi_-)^2 (v\pi_+)^2}{\gamma_1^4} - 2\Delta \frac{(v\pi_-)(v\pi_+)}{\gamma_1^2} \\ &= \frac{(\hbar\omega_0)^2}{4\varepsilon_0} \left[\left(\hat{n} + \frac{1}{2} + \xi \right)^2 - \frac{1}{4} \right] \\ &\quad - \hbar\omega_0 \left(\hat{n} + \frac{1}{2} + \frac{\xi}{2} \right), \end{aligned} \tag{39}$$

where $\omega_0 = eB/(m_0 c)$. The pseudospin Zeeman energy, i.e., half the energy difference between $\xi = \pm$, is transformed to

$$E_{\mathrm{Zeeman}} = \xi \frac{e\hbar}{m_0 c} \left(\frac{\pi^2}{p_0^2} - \frac{1}{2} \right) B, \tag{40}$$

which coincides with $-m_c \cdot B$ in the limit of $B = 0$.

The first and second terms in Eq. (39) correspond to p^4 and p^2 terms in the zero-field Hamiltonian, respectively, and become dominant when $\hbar\omega_0(n + 1/2) \gg \varepsilon_0$ and $\ll \varepsilon_0$, respectively. In the lower Landau levels where the second term dominates, the nth level at valley K_+ and the $(n+1)$-th level at K_- approximately degenerate. In higher levels where the first term becomes dominant, the nth Landau level at valley K_+ and the $(n+2)$-th level of K_- degenerate. Figure 1(b) plots the Landau level energy of Eq. (39) as a function of the magnetic field, where dashed and solid lines represent the valleys $\xi = +$ and $-$, respectively. At $\Delta = 0.1$ eV, for instance, the magnetic field corresponding to $\hbar\omega_0/\varepsilon_0 = 1$ is 7.6 T. A pair of dotted slopes represents the energy of the band bottom shifted by pseudospin Zeeman energy, i.e., $-\varepsilon_0 + \xi\hbar\omega_0/2$. In a small B field, they actually serve as the envelope curves for Landau levels of $\xi = \pm$. Full valley polarization occurs below the upper slope.

V. ABC MULTILAYER GRAPHENES

For the structure of bulk graphite, there are two known forms called ABA (AB, hexagonal, or Bernal) and ABC (rhombohedral) with different stacking manners.[18–20] The ABA phase is thermodynamically stable and common, while it is known that some portion of natural graphite takes the ABC form.[18] The low-energy band structure of a finite ABC graphene multilayer is given by a pair of surface bands localized at the outermost layers,[37,50,51] and the interlayer potential asymmetry opens an energy gap between those bands.[51–54]

Now, we attempt to argue about the chiral magnetic moment of gapped low-energy bands of ABC N-layered graphene in a parallel way to the bilayer graphene. If the basis is taken as $|A_1\rangle, |B_1\rangle$; $|A_2\rangle, |B_2\rangle$; $\ldots$; $|A_N\rangle, |B_N\rangle$, the low-energy effective Hamiltonian can be written as[37,50,51,53,54]

$$\mathcal{H}_{\mathrm{ABC}} = \begin{pmatrix} H_1 & V & & & \\ V^\dagger & H_2 & V & & \\ & V^\dagger & H_3 & V & \\ & & \ddots & \ddots & \ddots \end{pmatrix}, \tag{41}$$

and

$$H_j = \begin{pmatrix} U_j & vp_- \\ vp_+ & U_j \end{pmatrix}, \qquad V = \begin{pmatrix} 0 & 0 \\ \gamma_1 & 0 \end{pmatrix}, \tag{42}$$

where U_j is the electrostatic potential at the jth layer. For simplicity, we neglected the trigonal warping effect due to the extra band parameter.[54]

The potential asymmetry U_j can be induced by applying an electric field $\mathcal{E}$ perpendicular to the layer. When $\mathcal{E}$ is uniform,

the potential energy with respect to the middle of the stack is written as

$$U_j = \left(\frac{N+1}{2} - j\right) e\mathcal{E}d, \tag{43}$$

where $d \approx 0.334$ nm is the interlayer spacing. The bilayer graphene of Eq. (25) is a special case of Eq. (41) with $N = 2$ and $e\mathcal{E}d = 2\Delta$. The actual field $\mathcal{E}$ can be smaller than the externally applied electric field due to the screening by the electrons in the graphene.[51] We assume $\mathcal{E} > 0$ and $|U_j| \ll \gamma_1$ in the following.

At $p = 0$, there are two low-energy eigenenergies at $\varepsilon = U_1$ and U_N originating from $|A_1\rangle$ and $|B_N\rangle$, while all other states appear near $\varepsilon = \pm\gamma_1$ through the dimerization between $|B_j\rangle$ and $|A_{j+1}\rangle$ for each $j = 1, \ldots, N-1$. The effective Hamiltonian for the states near $\varepsilon = U_1$ is derived as

$$\begin{aligned}\mathcal{H}^{(\mathrm{eff})}(\mathbf{p}) &\approx \frac{\gamma_1^2}{(N-1)e\mathcal{E}d}\left(\frac{vp}{\gamma_1}\right)^{2N} - e\mathcal{E}d\left(\frac{vp}{\gamma_1}\right)^2 \\ &\equiv \frac{1}{N}\frac{p_0^2}{2m_0}\left(\frac{p}{p_0}\right)^{2N} - \frac{p^2}{2m_0},\end{aligned} \tag{44}$$

where the energy is measured from $\varepsilon = U_1$ and

$$m_0 = \frac{\gamma_1^2}{2v^2(e\mathcal{E}d)}, \qquad p_0 = \frac{\gamma_1}{v}\left(\sqrt{\frac{N-1}{N}}\frac{e\mathcal{E}d}{\gamma_1}\right)^{1/(N-1)}. \tag{45}$$

The term with p^2 comes from the direct coupling with the neighboring dimers formed by $|B_1\rangle$ and $|A_2\rangle$, and the p^{2N} term is from the Nth-order coupling with the other low-energy state of $|B_N\rangle$. All other terms are neglected in low energies as long as $vp_0/\gamma_1 \ll 1$. The band minimum appears at $p = p_0$ and energy $\varepsilon = -\varepsilon_0$, where

$$\varepsilon_0 = \frac{N-1}{N}\frac{p_0^2}{2m_0}. \tag{46}$$

The density of states diverges at $\varepsilon = -\varepsilon_0$ as

$$D(\varepsilon) \approx g_s g_v \frac{m_0}{\pi\hbar^2}\frac{1}{\sqrt{2N}}\frac{N}{N-1}\frac{1}{\sqrt{1+\varepsilon/\varepsilon_0}}. \tag{47}$$

For example, we show the energy dispersion of $N = 3$ and 4 in Fig. 2(a). Note that units p_0 and ε_0 depend on N. At $e\mathcal{E}d = 0.2$ eV, for instance, the characteristic energy scale is $\varepsilon_0 = 54$ meV and is 86 meV for $N = 3$ and 4, respectively.

The magnetization of Eq. (14) becomes

$$\begin{aligned}m = &-\frac{e}{2c}(xv^{y(\mathrm{eff})} - yv^{x(\mathrm{eff})}) \\ &-\xi\frac{e\hbar}{m_0 c}\left[\frac{N}{2}\left(\frac{p}{p_0}\right)^{2(N-1)} - \frac{1}{2}\right],\end{aligned} \tag{48}$$

where the second term m_c is the valley magnetic moment. The valley-splitting energy at the band bottom can be estimated by inserting $p = p_0$,

$$2|m_c(p_0)|\, B = (N-1)\hbar\omega_0, \tag{49}$$

where $\omega_0 = eB/(m_0 c)$. The splitting is greater for larger N under the same electric field $\mathcal{E}$. The condition for full valley polarization in the low B-field limit is

$$n < n_{\mathrm{crit}} = g_s\frac{1}{\pi}\sqrt{\frac{eB}{c\hbar}}\frac{\gamma_1}{\hbar v}\left(\sqrt{\frac{N-1}{N}}\frac{e\mathcal{E}d}{\gamma_1}\right)^{1/(N-1)}. \tag{50}$$

In the small-field region $e\mathcal{E}d \ll \gamma_1$, which is currently assumed, n_{crit} increases for larger N, i.e., the valley polarization is achieved up to higher electron densities in the larger stack. In the large N limit, n_{crit} approaches a value independent of $\mathcal{E}$,

$$n_{\mathrm{crit}}^{\infty} = g_s\frac{1}{\pi}\sqrt{\frac{eB}{c\hbar}}\frac{\gamma_1}{\hbar v}, \tag{51}$$

which approximates 1.5×10^{12} cm^{-2} at $B = 1$ T.

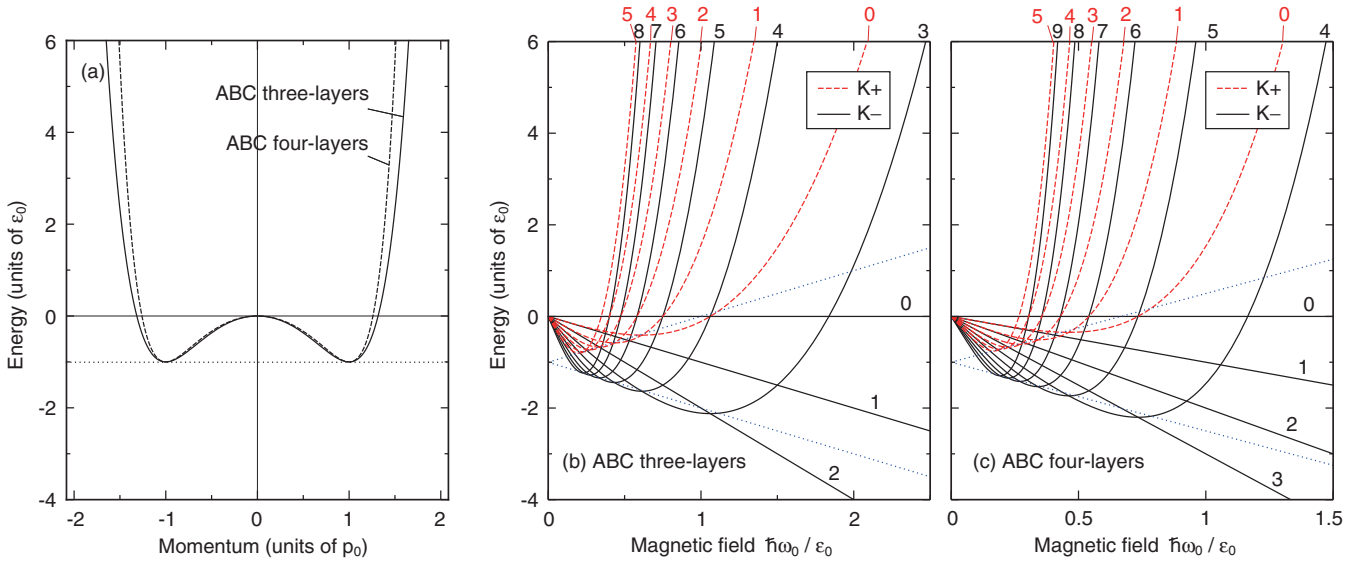

FIG. 2. (Color online) (a) Low-energy dispersion of gapped three- and four-layer ABC graphene given by Eq. (44). (b) and (c) Corresponding Landau level spectrum of Eq. (52) with some small n's, plotted against the magnetic field. A pair of dotted slopes represents $-\varepsilon_0 \pm \hbar(N-1)\omega_0/2$.

The low-energy Landau level spectrum near $\varepsilon = U_1$ is

$$\mathcal{H}^{(\mathrm{eff})} \approx \frac{\gamma_1^2}{(N-1)e\mathcal{E}d}\frac{(v\pi_-)^N(v\pi_+)^N}{\gamma_1^{2N}} - e\mathcal{E}d\frac{v\pi_-}{\gamma_1}\frac{v\pi_+}{\gamma_1}$$
$$= \frac{(N-1)^{N-1}}{N^N}\frac{(\hbar\omega_0)^N}{\varepsilon_0^{N-1}}\prod_{j=1}^{N}\left[\hat{n}+j-\frac{1-\xi}{2}N\right]$$
$$-\hbar\omega_0\left(\hat{n}+\frac{1}{2}+\frac{\xi}{2}\right). \tag{52}$$

Again, the valley splitting in the limit of $B = 0$ is shown to be equivalent to $-m_c \cdot B$ of Eq. (48). In higher Landau levels where the first term becomes dominant, the nth Landau level at valley K_+ and the $(n+N)$-th level of K_- degenerate. Figures 2(b) and 2(c) plot the Landau level spectra of Eq. (52) for the cases of $N = 3$ and 4, respectively. The Landau levels in small magnetic fields are well bound by dotted lines or the energies of $-\varepsilon_0 + \xi\hbar\omega_0/2$. At $e\mathcal{E}d = 0.2$ eV, for instance, the magnetic field corresponding to $\hbar\omega_0/\varepsilon_0 = 1$ is 33 and 52 T for $N = 3$ and 4, respectively. As argued above, we can see that, for greater N, the full valley polarization is possible up to a greater electron density (i.e., more Landau levels) at the same magnetic field.

VI. PSEUDOSPIN PARAMAGNETISM

The pseudospin Zeeman splitting causes the Pauli paramagnetism in an analogous way to a real spin. The magnetic susceptibility was calculated previously for gapped monolayer and bilayer graphenes,[8] and it was shown that the susceptibility in the quadratic dispersion near the $K_\pm$ point was expressed as a sum of valley pseudospin paramagnetism and Landau diamagnetism similar to a bare electron. In monolayer graphene, the pseudospin paramagnetism diverges in the zero gap limit, leading to a singular orbital susceptibility where the strong diamagnetism suddenly disappears off the Dirac point.[8,33,55–60]

Here, we extend the argument to general electronic structures other than quadratic and show that the pseudospin splitting always accompanies a paramagnetic contribution in any part of the dispersion. Let us consider a system in a magnetic field B with the Landau level sequence,

$$\varepsilon_n = \varepsilon(x_n,\delta) \qquad (n = 0,1,2,\ldots),$$
$$x_n = \left(n+\frac{1}{2}\right)\delta, \qquad \delta = \hbar\omega_c = \frac{\hbar eB}{m^*c}, \tag{53}$$

where n is the Landau level index and m^* is the effective mass characterizing the system. The second argument δ in $\varepsilon(x_n,\delta)$ represents the dependence on B, which is not included in x_n. For example, the low-energy Landau level of gapped monolayer graphene, Eq. (21), is given by

$$\varepsilon(x_n,\delta) = x_n + \frac{\xi}{2}\delta, \tag{54}$$

and that of bilayer graphene, Eq. (39), is given by

$$\varepsilon(x_n,\delta) = \frac{1}{4\varepsilon_0}\left[(x_n+\xi\delta)^2 - \frac{1}{4}\delta^2\right] + \left(x_n+\frac{\xi\delta}{2}\right), \tag{55}$$

with m^* replaced by m_0.

By treating $x(=x_n)$ and δ as independent variables, we can expand $\varepsilon(x,\delta)$ as

$$\varepsilon(x,\delta) = \varepsilon^{(0)}(x) + \varepsilon^{(1)}(x)\delta + \tfrac{1}{2}\varepsilon^{(2)}(x)\delta^2 + \cdots. \tag{56}$$

The zeroth-order term $\varepsilon^{(0)}$ is related to the energy spectrum at $B = 0$. In particular, when the system is isotropic, the dispersion is given by $\varepsilon^{(0)}(x)$ with $x = p^2/2m^*$. The first-order shift $\varepsilon^{(1)}\delta$ can be regarded as a pseudospin Zeeman term associated with magnetic moment $-(e\hbar/cm^*)\varepsilon^{(1)}$, which corresponds to m_c in previous arguments.

The thermodynamic potential becomes

$$\Omega = -\frac{1}{\beta}\frac{1}{2\pi l_B^2}\sum_{n=0}^{\infty}\varphi[\varepsilon(x_n,\delta)]$$
$$= -\frac{1}{\beta}\frac{m^*}{2\pi\hbar^2}\left[\int_0^\infty \varphi[\varepsilon(x,\delta)]dx + \frac{\delta^2}{24}\frac{\partial\varphi[\varepsilon(x,0)]}{\partial x}\bigg|_{x=0}\right]$$
$$+O(\delta^3), \tag{57}$$

where $\varphi(\varepsilon) = \ln[1+e^{-\beta(\varepsilon-\mu)}]$, $\beta = 1/(k_BT)$, μ is the chemical potential, and we used the Euler-Maclaurin formula in the second equation. Using Eq. (56), we can further expand Ω in terms of $\delta \propto B$. The magnetization is given by

$$M = -\left(\frac{\partial\Omega}{\partial B}\right)_\mu, \tag{58}$$

and the magnetic susceptibility is given by

$$\chi = -\left(\frac{\partial^2\Omega}{\partial B^2}\right)_\mu\bigg|_{B=0}. \tag{59}$$

We end up with

$$\chi(\mu,T) = \int_{-\infty}^{\infty} d\varepsilon\left(-\frac{\partial f}{\partial\varepsilon}\right)\chi(\varepsilon), \tag{60}$$

where

$$\chi(\varepsilon) = \left(\frac{e\hbar}{cm^*}\right)^2\left[D(\varepsilon)(\varepsilon^{(1)})^2 - \int^{\varepsilon} d\varepsilon\, D(\varepsilon)\varepsilon^{(2)}\right.$$
$$\left.-\frac{1}{12}\frac{m^*}{2\pi\hbar^2}\theta[\varepsilon-\varepsilon^{(0)}(0)]\frac{\partial\varepsilon^{(0)}(x)}{\partial x}\bigg|_{x=0}\right], \tag{61}$$

and $f(\varepsilon) = [1+e^{\beta(\varepsilon-\mu)}]^{-1}$ is the Fermi distribution function. In Eq. (61), $\varepsilon^{(1)}$ and $\varepsilon^{(2)}$ are regarded as functions of energy ε through $\varepsilon = \varepsilon^{(0)}(x)$. $D(\varepsilon)$ is the density of states given by

$$D(\varepsilon) = \frac{m^*}{2\pi\hbar^2}\int_0^\infty \delta[\varepsilon-\varepsilon^{(0)}(x)]dx. \tag{62}$$

The susceptibility at $T = 0$ is given by $\chi(\mu)$. The first term in Eq. (61) is regarded as the Pauli paramagnetism induced by the pseudospin magnetic moment. It always is positive and is determined purely by the density of states and the magnetic moment at Fermi energy. The second term is the summation of the second-order energy shift $\varepsilon^{(2)}$ over all the states below Fermi level, and the third term gives a discrete jump at the energy corresponding to $p = 0$.

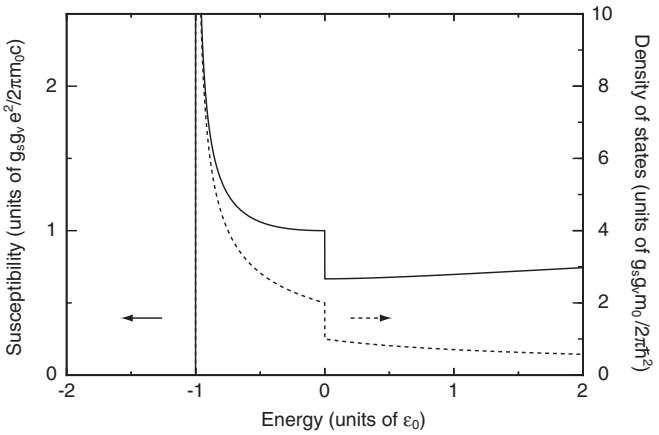

FIG. 3. Susceptibility (solid line) and density of states (dashed line) near the band bottom of asymmetric bilayer graphene, plotted against the Fermi energy.

For the low-energy spectrum of the gapped monolayer graphene, Eq. (54), we obtain[8]

$$\chi = \chi_P + \chi_L,$$
$$\chi_P = D\mu_B^{*2}, \qquad \chi_L = -\tfrac{1}{3} D\mu_B^{*2}, \tag{63}$$

where χ_P and χ_L come from the first and third terms in Eq. (61), respectively, and the second term is zero. Here, $D = g_s g_v m/(2\pi\hbar^2)\theta(\varepsilon)$ is the density of states, and $\mu_B^* = e\hbar/(2m^*c)$ is the effective Bohr magneton. Obviously, χ_P and χ_L correspond to conventional Pauli paramagnetism and Landau diamagnetism, respectively. The susceptibility calculated above is the contribution from the conduction band, while the valence band gives the exact opposite jump at the valence-band top. The total susceptibility is diamagnetic at $\chi = -\chi_P - \chi_L$ in the gap region and disappears in conduction and valence bands.[8]

For gapped bilayer graphene, Eq. (55), we get

$$\chi(\varepsilon) = \frac{g_s g_v e^2}{2\pi m_0 c^2} \times \begin{cases} 0 & (\varepsilon < -\varepsilon_0), \\ \dfrac{1}{2}\dfrac{2+\varepsilon/\varepsilon_0}{\sqrt{1+\varepsilon/\varepsilon_0}} & (-\varepsilon_0 < \varepsilon < 0), \\ \dfrac{1}{4}\dfrac{2+\varepsilon/\varepsilon_0}{\sqrt{1+\varepsilon/\varepsilon_0}} + \dfrac{1}{6} & (\varepsilon > 0). \end{cases} \tag{64}$$

The susceptibility diverges at the band bottom $\varepsilon = -\varepsilon_0$.[8] The physical meaning of the divergence is obvious, since the Pauli paramagnetism, i.e., the first term of Eq. (61) is proportional to the density of states, which diverges at the band bottom. The susceptibility of Eq. (64) is plotted in Fig. 3 together with the density of states, Eq. (31).

The argument can be extended to ABC N-layer graphene in a straightforward fashion. Using Eqs. (47) and (48), the pseudospin paramagnetic susceptibility above and near the band bottom $\varepsilon = -\varepsilon_0$ is written as

$$\chi(\varepsilon) \approx D(\varepsilon) m_c^2 = \frac{g_s g_v e^2}{2\pi m_0 c^2} \frac{N(N-1)}{2\sqrt{2N}} \frac{1}{\sqrt{1+\varepsilon/\varepsilon_0}}, \tag{65}$$

where m_0 and ε_0 are defined in Eqs. (45) and (46), respectively. The paramagnetic divergence is stronger for greater N.

VII. SPACE-DEPENDENT HALL CONDUCTIVITY

If the system is modulated by an external scalar potential, the anomalous current term gives a response current in an analogous way to the Hall effect. Here, we argue about the relation of the associated Hall conductivity to the anomalous magnetic moment. In graphenes, the Hall current exactly cancels between two valleys due to the time-reversal symmetry, and the real current appears only when the valley populations are differentiated, such as the Pauli paramagnetism. In the odd-valley case, such as the surface states of a strong topological insulator, it directly gives a net current and causes a magnetoelectric response.[21,22]

We consider a current distribution in a finite and isolated system modulated by an external potential $V(\mathbf{r})$. In the current densities of gapped monolayer and bilayer graphenes, given by Eqs. (18) and (32), respectively, the first term cancels in summation over the occupied states because it reverses the effective time-reversal operation $F \to F^*$. Then, the total current is given by a summation of the chiral term $c\nabla \times \boldsymbol{\mu}(\mathbf{r})$ as

$$\mathbf{J}(\mathbf{r}) = c\nabla \times \mathbf{M}(\mathbf{r}),$$
$$\mathbf{M}(\mathbf{r}) = \sum_{\text{occupied}} \boldsymbol{\mu}(\mathbf{r}). \tag{66}$$

When the potential $V(\mathbf{r})$ is weak and slowly varying, the Thomas-Fermi approximation gives

$$M(\mathbf{r}) \approx M_F - \frac{\partial M_F}{\partial \varepsilon_F} V(\mathbf{r}), \tag{67}$$

where M_F is the total magnetization of a uniform system,

$$M_F = \frac{1}{(2\pi\hbar)^2} \int_{\text{occupied}} m_c(p) d^2\mathbf{p}, \tag{68}$$

and $m_c(p)$ is the anomalous magnetic moment at momentum p. Then, Eq. (66) becomes

$$\mathbf{J}(\mathbf{r}) = ce \frac{\partial M_F}{\partial \varepsilon_F} [\mathbf{e}_z \times \mathbf{E}(\mathbf{r})], \tag{69}$$

where $\mathbf{E}(\mathbf{r}) = -\nabla V(\mathbf{r})/(-e)$ is the electric field, leading to a response function,

$$\sigma_{xy} = -ce \frac{\partial M_F}{\partial \varepsilon_F}. \tag{70}$$

By applying Eq. (70) to the conduction-band electrons of gapped monolayer graphene, where $m_c(p)$ is given by the second term in Eq. (20), we have

$$\sigma_{xy} = \xi \frac{e^2}{2h}. \tag{71}$$

For gapped N-layer ABC graphenes, including the bilayer, of which $m_c(p)$ is given by the second term in Eq. (48), the expression approximates in high energies $\varepsilon \gg \varepsilon_0$ as

$$\sigma_{xy} \approx \xi \frac{Ne^2}{2h}. \tag{72}$$

When the system is confined to a finite space, the above-mentioned Hall current gives a chiral edge current at the

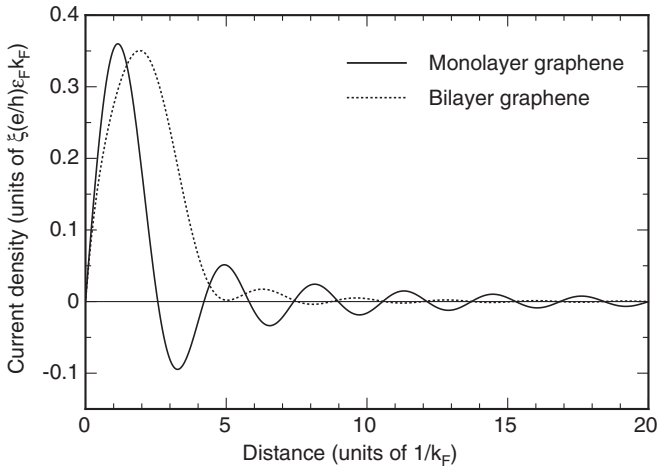

FIG. 4. Single-valley current distribution contributed by conduction-band electrons of gapped monolayer (solid curve) and bilayer graphenes (dashed curve), terminated at $x = 0$.

boundary. When the confining potential is slowly varying in space, the current circulation is

$$I = -\frac{1}{e}\int^{\varepsilon_F} \sigma_{xy}(\varepsilon)d\varepsilon = cM_F, \tag{73}$$

as a natural consequence. This is equally true in a sharp potential as well, where the current is distributed in a range of the Fermi wavelength from the boundary. Figure 4 illustrates the single-valley current distribution given by the conduction-band electrons of gapped monolayer and bilayer graphenes. The details of the derivation are presented in the Appendix.

From its definition, the Hall conductivity argued here, Eq. (70), is the long-wavelength limit of the static Hall conductivity, namely, $\lim_{q\to 0}\lim_{\omega\to 0}\sigma_{xy}(q,\omega)$. For the original Hamiltonian of monolayer graphene, Eq. (15), this is evaluated as[61]

$$\lim_{q\to 0}\lim_{\omega\to 0}\sigma_{xy}(q,\omega) = -\xi\frac{e^2}{2h}\theta(\Delta - |\varepsilon_F|), \tag{74}$$

where $\theta(x) = 1$ $(x > 0)$, 0 $(x < 0)$ is the step function and $\Delta > 0$ is assumed here. The low-energy result, Eq. (71), describes the contribution from the conduction-band electrons and, indeed, coincides with the discontinuous jump at $\varepsilon = \Delta$ in Eq. (74). The valence band gives an exactly opposite jump at $\varepsilon = -\Delta$ so that we have the half-integer Hall conductivity inside the gap and zero in the conduction and valance bands.

Note that usual Hall conductivity, relevant in the transport, is given by a different limit, $\lim_{\omega\to 0}\lim_{q\to 0}\sigma_{xy}(q,\omega)$. This is calculated for gapped monolayer graphene as[62]

$$\lim_{\omega\to 0}\lim_{q\to 0}\sigma_{xy}(q,\omega) = \begin{cases} -\xi\dfrac{e^2}{2h}\dfrac{\Delta}{|\varepsilon_F|} & (|\varepsilon_F| > \Delta), \\ -\xi\dfrac{e^2}{2h} & (|\varepsilon_F| < \Delta), \end{cases} \tag{75}$$

which differs from Eq. (74) except for the value inside the gap. The Berry curvature is directly related to this transport Hall conductivity.[13,63]

From the relationship between the local current and the local magnetic moment, Eq. (66), the spatial-dependent static Hall conductivity $\sigma_{xy}(q)$ can be formulated as a magnetization-density correlation function, i.e.,

$$M(q) = \frac{1}{e}\sigma_{xy}(q)V(q). \tag{76}$$

In the low-energy region of gapped monolayer graphene, it becomes a density-density correlation function because the pseudospin magnetization, Eq. (20), is constant for each eigenstate regardless of the details of the wave function. This suggests that $\sigma_{xy}(q)$ is insensitive to the disorder localization effect since the magnetic moment of each eigenstate remains even when the wave function is localized. This is in contrast to the transport Hall conductivity, where the localized eigenstates have zero contribution.

Last, we show that Hall conductivity, Eq. (70), is directly related to index difference Δn between degenerated Landau levels of two valleys, which are argued about in the previous sections. This is defined by the ratio of pseudospin Zeeman splitting to Landau level spacing, or

$$\Delta n = \frac{2m_c B}{\hbar\omega_c},$$
$$\hbar\omega_c = \frac{\hbar eB}{c}2\pi\left(\frac{\partial S(\varepsilon_F)}{\partial\varepsilon_F}\right)^{-1}, \tag{77}$$

and $S(\varepsilon_F) = \pi p_F^2$ is the area of the momentum space at the Fermi energy ε_F. Using Eqs. (68) and (70), we obtain

$$\Delta n = \frac{2hc}{e}\frac{\partial M_F}{\partial\varepsilon_F} = -\frac{2h}{e^2}\sigma_{xy}. \tag{78}$$

Indeed, we have $\Delta n = 1$ for gapped monolayer graphene and $\Delta n \approx N$ for gapped N-layer ABC graphene (including bilayer graphene) in high energies.

VIII. CONCLUSION

We presented systematic analyses of the anomalous chiral current and magnetic moment in gapped graphenes and related materials. Starting from the low-energy effective-mass theory, we formulated a description of local current distribution supporting anomalous magnetic moment in general Bloch systems. In gapped monolayer, bilayer, and ABC multilayer graphenes, we showed that the chiral current circulation accounted for the valley-dependent magnetic moment and valley splitting of Landau levels. The bilayer and ABC multilayer graphenes exhibit a large paramagnetism at the band bottom, and full valley polarization is possible in relatively high electron densities.

Various mechanisms for valley polarization or valley filtering have been suggested, which might be used to control electronic devices.[6,7,64–67] The possibility of full valley polarization in a graphene bilayer and ABC multilayers invokes a simple mechanism for valley-dependent transport. For example, if we could locally apply opposite magnetic fields to the left and right sides of a gapped bilayer or ABC-multilayer strip and could achieve different valley polarizations in two regions, then the transport between two regions would be killed, as long as the valley flipping is prohibited in the intermediate

region, i.e., the impurity potential and the spacial magnetic field change are smooth compared to the atomic scale. On the contrary, electrons can travel almost freely when the same magnetic field is applied to two regions.

While we focus on the family of ABC-stacked multilayer graphenes in the present paper, the anomalous magnetic moment arises in ABA-stacked multilayer graphenes as well when the inversion symmetry is broken.[49] In ABA multilayers with an odd number of layers, the lattice structure originally is lacking in the inversion symmetry so that the valley splitting intrinsically exists even in the absence of the external field.[68] The present analysis applies to every sub-band comprising the total band structure, each of which is akin to gapped monolayer or bilayer graphenes.[68,69]

ACKNOWLEDGMENT

This project has been funded by JST-EPSRC Japan-UK Cooperative Programme Grant No. EP/H025804/1.

APPENDIX: CHIRAL EDGE CURRENT

Here, we calculate the edge current distribution of gapped monolayer and bilayer graphenes bound by a sharp confining potential. Let us consider a low-energy Hamiltonian gapped monolayer graphene, Eq. (16), bound by a potential barrier,

$$V(x) = \begin{cases} \infty & (x < 0), \\ 0 & (x > 0). \end{cases} \tag{A1}$$

The eigenstates are given by

$$F(\mathbf{r}) \propto e^{ik_y y} \sin k_x x. \tag{A2}$$

The current density of Eq. (18), integrated over the occupied states, is written in terms of the Bessel function as

$$J_y(\mathbf{r}) = \xi \frac{e}{h} \frac{\varepsilon_F}{x} J_2(2k_F x). \tag{A3}$$

It oscillates and decays in the length scale of $2\pi/k_F$ as shown in Fig. 4. The total edge current is

$$I \equiv \int_0^\infty dx\, J_y(\mathbf{r}) = \xi \frac{e}{2h} \varepsilon_F, \tag{A4}$$

which coincides with cM_F.

A similar argument is available in bilayer graphene. For simplicity, we consider high energies $\varepsilon \gg \varepsilon_0$ and neglect the p^2 term in Eq. (27). The Schrödinger equation becomes the fourth-order differential equation due to the p^4 term, and the boundary condition becomes $F(0) = F'(0) = 0$. The eigenstate then becomes

$$F(\mathbf{r}) \propto e^{ik_y y}[\cos k_x x + \sin k_x x - e^{-k_x x}]. \tag{A5}$$

The total current density, Eq. (34), integrated over the occupied states, is numerically calculated and is plotted in Fig. 4. Again, the length scale is characterized by its Fermi wavelength, but it decays more rapidly than in the monolayer. The total edge current is shown to be

$$I = \int_0^\infty dx\, J_y(\mathbf{r}) = \xi \frac{e}{h} \varepsilon_F, \tag{A6}$$

which is twice as large as the monolayer's.

[1] Y. Yafet, *Solid State Physics: Advances in Research and Applications* (Academic, New York, 1963), Vol. 14.
[2] C. Kittel, *Quantum Theory of Solids* (Wiley, New York, 1963).
[3] K. S. Novoselov, A. K. Geim, S. V. Morozov, D. Jiang, Y. Zhang, S. V. Dubonos, I. V. Grigorieva, and A. A. Firsov, Science **306**, 666 (2004).
[4] K. S. Novoselov, A. K. Geim, S. V. Morozov, D. Jiang, M. I. Katsnelson, I. V. Grigorieva, S. V. Dubonos, and A. A. Firsov, Nature (London) **438**, 197 (2005).
[5] Y. Zhang, Y.-W. Tan, H. L. Stormer, and P. Kim, Nature (London) **438**, 201 (2005).
[6] D. Xiao, W. Yao, and Q. Niu, Phys. Rev. Lett. **99**, 236809 (2007).
[7] W. Yao, D. Xiao, and Q. Niu, Phys. Rev. B **77**, 235406 (2008).
[8] M. Koshino and T. Ando, Phys. Rev. B **81**, 195431 (2010).
[9] M.-C. Chang and Q. Niu, Phys. Rev. B **53**, 7010 (1996).
[10] D. Xiao, J. Shi, and Q. Niu, Phys. Rev. Lett. **95**, 137204 (2005).
[11] T. Thonhauser, D. Ceresoli, D. Vanderbilt, and R. Resta, Phys. Rev. Lett. **95**, 137205 (2005).
[12] D. Ceresoli, T. Thonhauser, D. Vanderbilt, and R. Resta, Phys. Rev. B **74**, 024408 (2006).
[13] D. Xiao, M.-C. Chang, and Q. Niu, Rev. Mod. Phys. **82**, 1959 (2010).
[14] K. S. Novoselov, E. McCann, S. V. Morozov, V. I. Falko, M. I. Katsnelson, U. Zeitler, D. Jiang, F. Schedin, and A. K. Geim, Nat. Phys. **2**, 177 (2006).
[15] T. Ohta, A. Bostwick, T. Seyller, K. Horn, and E. Rotenberg, Science **313**, 951 (2006).
[16] E. V. Castro, K. S. Novoselov, S. V. Morozov, N. M. R. Peres, J. M. B. Lopes dos Santos, J. Nilsson, F. Guinea, A. K. Geim, and A. H. Castro Neto, Phys. Rev. Lett. **99**, 216802 (2007).
[17] J. B. Oostinga, H. B. Heersche, X.-L. Liu, A. F. Morpurgo, and L. M. K. Vandersypen, Nature Mater. **7**, 151 (2008).
[18] H. Lipson and A. R. Stokes, Proc. R. Soc. London, Ser. A **181**, 101 (1942).
[19] R. R. Haering, Can. J. Phys. **36**, 352 (1958).
[20] J. W. McClure, Carbon **7**, 425 (1969).
[21] X.-L. Qi, T. L. Hughes, and S.-C. Zhang, Phys. Rev. B **78**, 195424 (2008).
[22] A. M. Essin, J. E. Moore, and D. Vanderbilt, Phys. Rev. Lett. **102**, 146805 (2009).
[23] M. Z. Hasan and C. L. Kane, Rev. Mod. Phys. **82**, 3045 (2010).
[24] X.-L. Qi and S.-C. Zhang, e-print arXiv:1008.2026v1.
[25] J. C. Slonczewski and P. R. Weiss, Phys. Rev. **109**, 272 (1958).
[26] D. P. DiVincenzo and E. J. Mele, Phys. Rev. B **29**, 1685 (1984).
[27] G. W. Semenoff, Phys. Rev. Lett. **53**, 2449 (1984).
[28] N. H. Shon and T. Ando, J. Phys. Soc. Jpn. **67**, 2421 (1998).

[29]Y. Zheng and T. Ando, Phys. Rev. B **65**, 245420 (2002).
[30]T. Ando, J. Phys. Soc. Jpn. **74**, 777 (2005).
[31]V. P. Gusynin and S. G. Sharapov, Phys. Rev. Lett. **95**, 146801 (2005).
[32]N. M. R. Peres, F. Guinea, and A. H. Castro Neto, Phys. Rev. B **73**, 125411 (2006).
[33]J. W. McClure, Phys. Rev. **104**, 666 (1956).
[34]S. Y. Zhou, G.-H. Gweon, A. V. Fedorov, P. N. First, W. A. de Heer, D.-H. Lee, F. Guinea, A. H. Castro Neto, and A. Lanzara, Nature Mater. **6**, 770 (2007).
[35]S. Y. Zhou, D. A. Siegel, A. V. Fedorov, F. El Gabaly, A. K. Schmid, A. H. Castro Neto, D.-H. Lee, and A. Lanzara, Nature Mater. **7**, 259 (2008).
[36]E. McCann and V. I. Falko, Phys. Rev. Lett. **96**, 086805 (2006).
[37]F. Guinea, A. H. Castro Neto, and N. M. R. Peres, Phys. Rev. B **73**, 245426 (2006).
[38]C. L. Lu, C. P. Chang, Y. C. Huang, J. M. Lu, C. C. Hwang, and M. F. Lin, J. Phys.: Condens. Matter **18**, 5849 (2006).
[39]C. L. Lu, C. P. Chang, Y. C. Huang, R. B. Chen, and M. L. Lin, Phys. Rev. B **73**, 144427 (2006).
[40]E. McCann, Phys. Rev. B **74**, 161403 (2006).
[41]M. Koshino and T. Ando, Phys. Rev. B **73**, 245403 (2006).
[42]J. Nilsson, A. H. Castro Neto, N. M. R. Peres, and F. Guinea, Phys. Rev. B **73**, 214418 (2006).
[43]B. Partoens and F. M. Peeters, Phys. Rev. B **74**, 075404 (2006).
[44]A. Misu, E. Mendez, and M. S. Dresselhaus, J. Phys. Soc. Jpn. **47**, 199 (1979).
[45]T. Ando and M. Koshino, J. Phys. Soc. Jpn. **78**, 034709 (2009).
[46]T. Ando and M. Koshino, J. Phys. Soc. Jpn. **78**, 104716 (2009).
[47]Y. Zhang, T.-T. Tang, C. Girit, Z. Hao, M. C. Martin, A. Zettl, M. F. Crommie, Y. R. Shen, and F. Wang, Nature (London) **459**, 820 (2009).
[48]K. F. Mak, C. H. Lui, J. Shan, and T. F. Heinz, Phys. Rev. Lett. **102**, 256405 (2009).
[49]M. Koshino and E. McCann, Phys. Rev. B **81**, 115315 (2010).
[50]J. L. Mañes, F. Guinea, and M. A. H. Vozmediano, Phys. Rev. B **75**, 155424 (2007).
[51]M. Koshino, Phys. Rev. B **81**, 125304 (2010).
[52]M. Aoki and H. Amawashi, Solid State Commun. **142**, 123 (2007).
[53]C. L. Lu, C. P. Chang, Y. C. Huang, J. H. Ho, C. C. Hwang, and M. F. Lin, J. Phys. Soc. Jpn. **76**, 024701 (2007).
[54]M. Koshino and E. McCann, Phys. Rev. B **80**, 165409 (2009).
[55]S. G. Sharapov, V. P. Gusynin, and H. Beck, Phys. Rev. B **69**, 075104 (2004).
[56]H. Fukuyama, J. Phys. Soc. Jpn. **76**, 043711 (2007).
[57]M. Nakamura, Phys. Rev. B **76**, 113301 (2007).
[58]M. Koshino and T. Ando, Phys. Rev. B **75**, 235333 (2007).
[59]A. Ghosal, P. Goswami, and S. Chakravarty, Phys. Rev. B **75**, 115123 (2007).
[60]M. Koshino, Y. Arimura, and T. Ando, Phys. Rev. Lett. **102**, 177203 (2009).
[61]A. W. W. Ludwig, M. P. A. Fisher, R. Shankar, and G. Grinstein, Phys. Rev. B **50**, 7526 (1994).
[62]N. A. Sinitsyn, A. H. MacDonald, T. Jungwirth, V. K. Dugaev, and J. Sinova, Phys. Rev. B **75**, 045315 (2007).
[63]D. J. Thouless, M. Kohmoto, M. P. Nightingale, and M. den Nijs, Phys. Rev. Lett. **49**, 405 (1982).
[64]A. Rycerz, J. Tworzydo, and C. W. J. Beenakker, Nat. Phys. **3**, 172 (2007).
[65]J. M. Pereira Jr., F. M. Peeters, R. N. Costa Filho, and G. A. Farias, J. Phys.: Condens. Matter **21**, 045301 (2009).
[66]D. S. L. Abergel and T. Chakraborty, Appl. Phys. Lett. **95**, 062107 (2009).
[67]T. Nakanishi, M. Koshino, and T. Ando, Phys. Rev. B **82**, 125428 (2010).
[68]M. Koshino and E. McCann, Phys. Rev. B **83**, 165443 (2011).
[69]M. Koshino and T. Ando, Solid State Commun. **149**, 1123 (2009).